Electrochemistry Communications 12 (2010) 374–377

Contents lists available at ScienceDirect

Electrochemistry Communications

journal homepage: www.elsevier.com/locate/elecom

Characterization of the 3-dimensional microstructure of a graphite negative electrode from a Li-ion battery

P.R. Shearing [a], L.E. Howard [b], P.S. Jørgensen [c], N.P. Brandon [a,*], S.J. Harris [d]

[a] Department of Earth Science and Engineering, Imperial College London, London, United Kingdom
[b] Department of Mineralogy, The Natural History Museum, South Kensington, London, United Kingdom
[c] Risø National Laboratory, Roskilde, Denmark
[d] General Motors R&D Centre, Warren, Michigan, USA

ARTICLE INFO

Article history:
Received 10 December 2009
Received in revised form 23 December 2009
Accepted 24 December 2009
Available online 4 January 2010

Keywords:
X-ray tomography
Microstructure
Representative volume element
Battery
Graphite electrode

ABSTRACT

The 3-dimensional microstructure of a porous electrode from a lithium-ion battery has been characterized for the first time. We use X-ray tomography to reconstruct a $43 \times 348 \times 478$ μm sample volume with voxel dimensions of 480 nm, subsequent division of the reconstructed volumes into sub-volumes of different sizes allow us to determine microstructural parameters as a function of sub-division size. We show that the minimum size for a representative volume element is about $43 \times 60 \times 60$ μm for volume-specific surface area, but as large as the full sample volume for porosity and tortuosity.

1. Introduction

Li-ion batteries are generally analyzed using a macro-homogeneous porous electrode model [1,2]. Model input includes particle radius and porosity; otherwise, it assumes that the electrode is an isotropic, homogeneous, 1-dimensional porous material constructed from mono-disperse, non-porous isotropic spherical particles small compared to the electrode thickness. This model has been highly successful in optimizing electrode properties such as film thickness and porosity [3].

The ability to predict cell degradation is a challenge, however, because so many seemingly unrelated degradation mechanisms have been identified [4]. Analysis of specific degradation mechanisms can in some cases provide a rationale for experimentally observed phenomena [5–8], but without additional experimental data, quantitative cause-and-effect relationships between observation and degradation pathway are difficult to develop. Measurements showing the evolution of the 3-dimensional microstructure will help enable deconvolution of these effects.

There are a number of experimental techniques that can provide such information. For example, Yoshizawa et al. [9] used electron tomography (3D TEM) to observe the internal structure and connectivity of carbon nanospheres. Thorat et al. [10] have developed a novel technique to determine electrode and separator tortuosity, in contrast to its more common treatment as an adjustable parameter [2].

The use of tomographic techniques in the field of fuel cell research has provided unprecedented access to microstructural information. Two commonly used techniques are high resolution X-ray computerized tomography [11] and focused ion beam tomography [12,13]. Of these, focused ion beam milling has been used to examine battery electrodes [14–19]; however, to date there have been no 3-dimensional reconstructions of a battery electrode presented.

This paper presents the results of tomography experiments to characterize graphite electrode microstructures with subsequent geometrical analysis of the reconstructed volume. Any tomography procedure must balance the dual requirements of reconstructing a sufficient sample volume while maintaining imaging resolution. The high stopping distance of ions in graphite means that graphite specimens are highly resistant to ion beam milling, thus limiting the sample volume that can be reconstructed. After preliminary investigations, X-ray nano-CT has been selected as the most appropriate technique to characterize our sample. As material failure is often a result of local inhomogeneities and defects [20,21], we focus here on the validity of the widely used assumptions of homogeneity and isotropy in battery electrode modeling.

* Corresponding author. Tel.: +44 2075945704.
E-mail address: n.brandon@imperial.ac.uk (N.P. Brandon).

1388-2481/$ - see front matter © 2009 Elsevier B.V. All rights reserved.
doi:10.1016/j.elecom.2009.12.038

2. Experimental

About 1 cm^2 from a graphite negative electrode was harvested from a Lishen 18650 battery of 2.2 A h capacity. The copper current collector was dissolved in nitric acid, and an area of the electrode was identified for examination and mounted onto an aluminum pin using silver paint. Dissolution of metals from carbon using nitric acid is a standard process (e.g. [22]).

The Gatan X-ray ultramicroscope (XuM) system was used for high resolution computerized tomography (nano-CT) [23,24]. Projected X-ray images were acquired at 1° rotation increments over 190° and reconstructed using Gatan's cone-beam back-projection algorithm to generate a 3D volume. The images were acquired with an 80 s exposure time (total acquisition time of 4.2 h) and a total magnification of 41.4×, corresponding to 480 nm voxel dimensions.

The total reconstructed sample volume was $43 \times 348 \times 478$ μm; subsequent geometrical analysis was conducted to extract porosity, pore-connectivity, particle and pore size distribution, surface area and tortuosity. The analysis considered the entire bulk volume as well as a number of sub-volumes (which, when combined, represent the entire bulk volume); sub-volume dimensions are provided in Table 1. We then extracted standard deviations at each sub-volume dimension, allowing us to suggest the minimum representative volume element (RVE) size.

Graphite surface area was calculated by creating polygons along the surface defined by the pore-graphite interface. Tortuosity is calculated based on the geometrical definition provided by Shen [25] and is determined as follows: for a given pore structure the minimum distance from one side to the other is termed "D". The shortest distances ($L1$) from every pixel on one side to the closest pixel on the opposing side is calculated, ensuring that the path is maintained within the 3-dimensional pore structure. Tortuosity, calculated for each of these $L1$ values is defined as tortuosity = $L1/D$, and tortuosity factor is defined as the square of tortuosity. Pore size distribution was calculated by the 3-dimensional "continuous PSD" method described in [26].

Table 1
Dimensions of sub-division levels.

Sub-division level	Z thickness (voxels)	X width (voxels)	Y depth (voxels)
Bulk	90	726	996
1	90	242	249
2	90	242	124
3	90	121	124
4	90	121	62
5	90	60	62
6	45	60	62
7	45	60	31
8	45	30	31
9	22	30	31

3. Results and discussion

Fig. 1a shows an individual "slice" from the reconstructed tomography sequence; Fig. 1b shows the rendered solid graphite

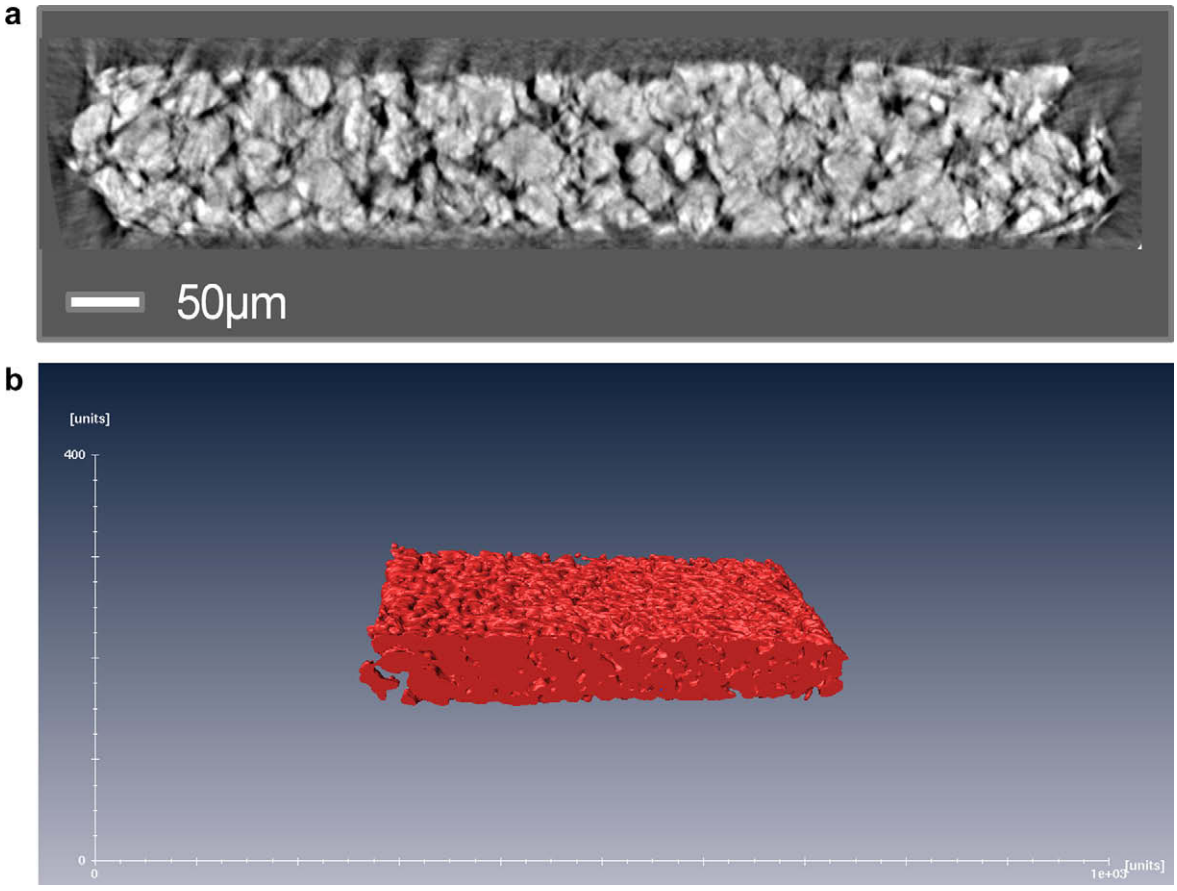

Fig. 1. (a) Individual slice from the tomography sequence. (b) Rendering of 300 individual tomography slices (dimensions $43 \times 348 \times 144$ μm).

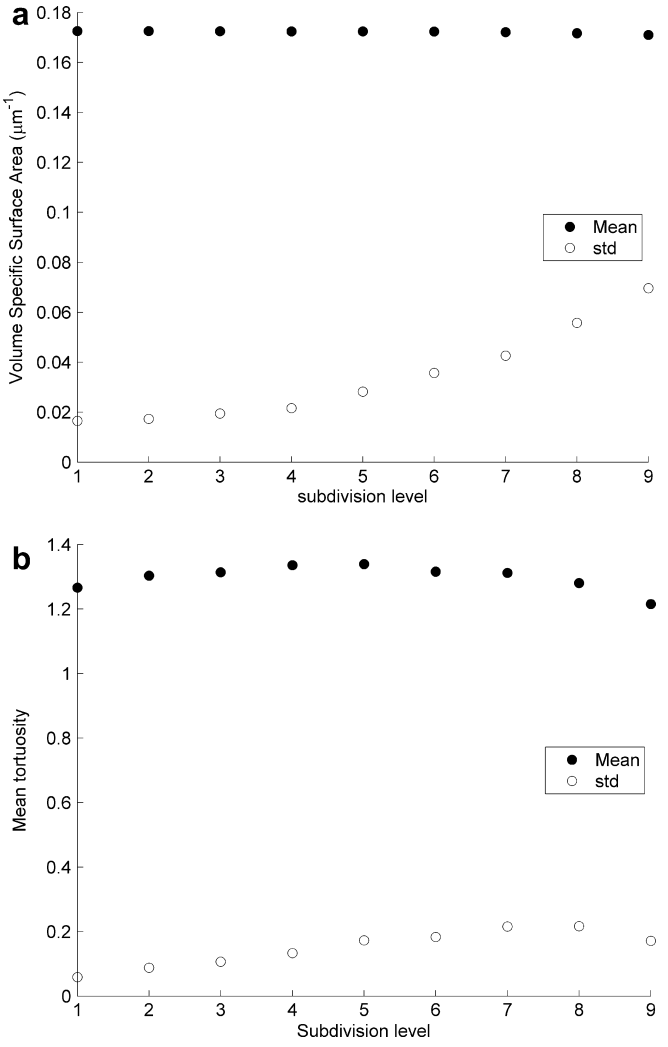

Fig. 2. (From left) (a) mean surface area per unit volume and standard deviation for sub-division levels 1–9. (b) Mean tortuosity and standard deviation for sub-division levels 1–9.

reconstruction (due to constraints in the rendering software, the image is only a partial reconstruction; geometrical analysis has been carried out using the sub-division geometries outlined in Table 1).

Geometrical analysis of the bulk sample gives a porosity of 15.4%, with more than 95% of pores percolating through the sample. We note that porosity is chosen by the manufacturer as a trade off between power and energy. High porosity corresponds to fast Li transport through the electrolyte and, therefore, high power. However, high porosity means less active material per unit volume and, therefore, lower capacity. The manufacturer has chosen to make this a high energy battery, and the measured value of 15.4% porosity is therefore in line with what might be expected for this case. The continuous PSD method [26] gives the median diameter of the graphite particle size distribution (d_{50}), as 4.78 μm and the pore d_{50} as 1.26 μm.

Fig. 2a shows the mean and standard deviation of the volume-specific surface area as a function of sub-division level. The mean value is independent of sub-division level since the volume-specific surface area averaged over all of the sub-divisions is independent of sub-division size. As expected, the standard deviation falls as the sub-division sizes become larger, tending to a constant value around sub-division level 3. Thus the minimum RVE size for this parameter is around level 3, with smaller volume elements more likely to give results that deviate significantly from the mean. The dimensions of such an RVE are significantly larger than those obtainable for this sample using FIB tomography.

Fig. 2b gives shows the variation of tortuosity with sub-division level, a tortuosity of 1.27 (tortuosity factor 1.60), measured at sub-division level 1. In this case, however, an increase in standard deviation of tortuosity is observed between sub-volumes 1 and 2, suggesting that the minimum RVE for this parameter is at least as large as sub-division level 1. A graph of porosity versus sub-division size suggests an intermediate minimum RVE.

Fig. 3 shows mosaic plots for porosity, volume-specific surface area and tortuosity. Each mosaic tile represents a mean value averaged over the tile area and through the electrode thickness; the figure emphasizes the extent of inhomogeneity at this scale. Arrows highlight a region that has low tortuosity, high volume-specific surface area and average porosity, contradicting a perhaps naïve view that these properties should scale together.

There are several strategies for defining tortuosity in 3-dimensions [27,28]. The simple measure of tortuosity used here is not sensitive to the presence of pore constrictions and therefore cannot accurately describe the influence of the geometrical constraints on transport. However, we believe that these data do provide qualitative information about resistance to transport. The Bruggeman relationship is derived theoretically for conduction in mixed media (e.g. diffusion in pores); this relationship is commonly used in the battery community to relate porosity and tortuosity (see. e.g. [10,29]). The generalized form of the Bruggeman relationship is:

$$\tau = \varepsilon^{1-\alpha}$$

where τ is tortuosity, ε is porosity and α is the Bruggeman exponent, usually assumed to be 1.5.

The Bruggeman relationship does not hold for our definition of tortuosity at sub-division level 3. In future work we will use finite element and Lattice Boltzmann methods to provide a more robust measure of the effect of the pore architecture on transport rates.

4. Conclusions

The use of high resolution X-ray CT has provided the first quantitative microstructural, 3-dimensional reconstruction of a Li-ion battery electrode. Several geometrical parameters were extracted, including porosity, tortuosity, surface area and pore and particle size distribution. The availability of highly detailed tomography data provides opportunities to test theoretically and empirically derived relationships, such as the Bruggeman relationship; and to learn how changes in electrode architecture correlate to changes in cell performance.

Acknowledgements

Paul Shearing wishes to acknowledge support from the UK EPSRC Supergen Programme.

Peter Jørgensen wishes to acknowledge financial support from The Danish Council for Strategic Research, via the SERC Project, Contract No. 2104-06-0011. The authors acknowledge EPSRC Grant GR/T26344 for access to image analysis and rendering software.

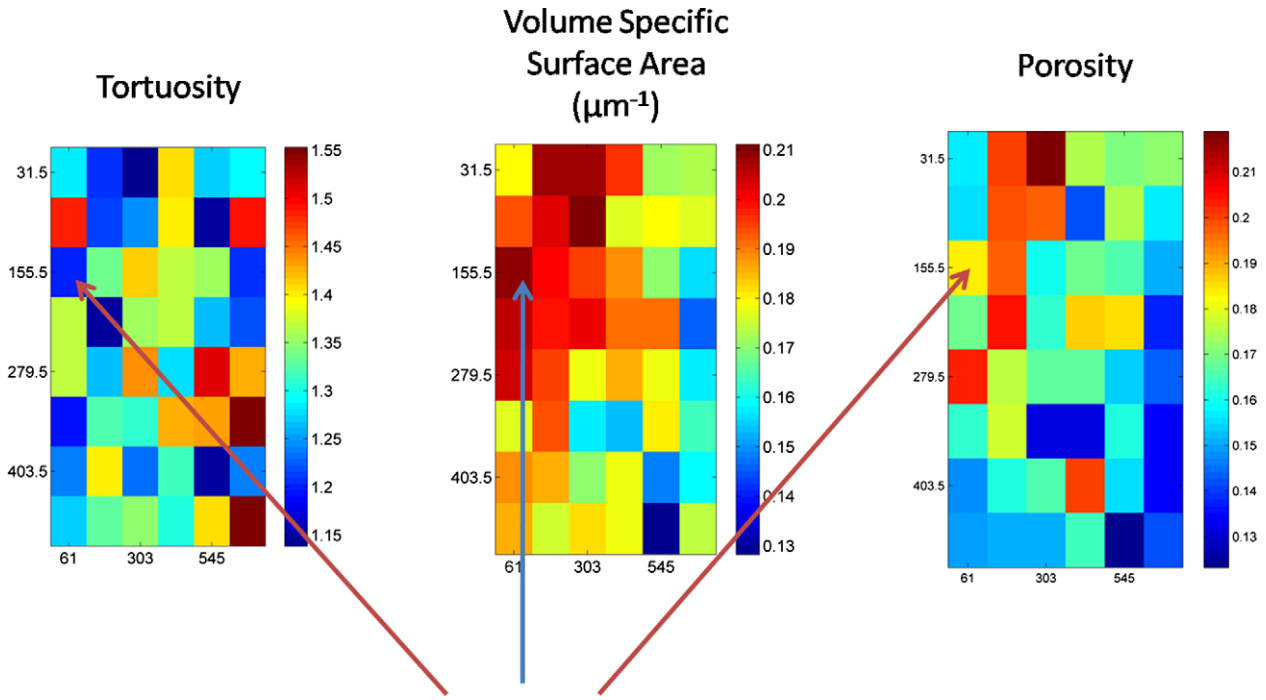

Fig. 3. Mosaic plots showing spatial distribution of tortuosity, surface area and porosity. Axes labeling refers to the co-ordinates of the voxel system. Arrows highlight a region that has low tortuosity, high volume-specific surface area and average porosity.

References

[1] M. Doyle, T. Fuller, J. Newman, J. Electrochem. Soc. 140 (1993) 1526.
[2] M. Doyle, J. Newman, A. Gozdz, C. Schmutz, J.M. Tarascon, J. Electrochem. Soc. 143 (1996) 1890.
[3] J. Newman, J. Electrochem. Soc. 142 (1995) 97.
[4] J. Vetter, P. Novak, M. Wagner, C. Veit, K. Moller, J. Besenhard, M. Winter, M. Wohlfahrt-Mehrens, C. Vogler, A. Hammouche, J. Power Sources 147 (2005) 269.
[5] P. Ramadass, B. haran, R. White, B. Popov, J. Power Sources 123 (2003) 230.
[6] G. Sikha, B. Popov, R. White, J. Electrochem. Soc. 151 (2004) A1104.
[7] S. Santhanagoplalan, Q. Guo, P. Ramadass, R. White, J. Power Sources 156 (2006) 620.
[8] R. Darling, J. Newman, J. Electrochem. Soc. 145 (1998) 990.
[9] N. Yoshizawa, O. Tanaike, H. Hatori, K. Yoshikawa, A. Kondo, T. Abe, Carbon 44 (2006) 2558.
[10] I. Thorat, D. Stephenson, N. Zacharias, K. Zaghib, J. Harb, D. Wheeler, J. Power Sources 188 (2009) 592.
[11] J.R. Izzo, A.S. Joshi, K.N. Grew, W.K.S. Chiu, A. Tkachuk, S.H. Wang, W.B. Yun, J. Electrochem. Soc. 155 (5) (2008) B504.
[12] P.R. Shearing, J.I. Golbert, R.J. Chater, N.P. Brandon, Chem. Eng. Sci., 2009, 10.1016/j.ces.2009.05.038.
[13] J.R. Wilson, W. Kobsiriphat, R. Mendoza, H.Y. Chen, J.M. Hiller, D.J. Miller, K. Thornton, P.W. Voorhees, S.B. Adler, S.A. Barnett, Nat. Mater. 5 (7) (2006) 541.
[14] H. Zhang, F. Li, C. Liu, J. Tan, H. Cheng, J. Phys. Chem. B 109 (2005) 22205.
[15] Y. Tian, A. Timmons, J.R. Dahn, J. Electrochem. Soc. 156 (2009) A187.
[16] A. Sano, M. Kurihara, T. Abe, Z. Ogumi, J. Electrochem. Soc. 156 (2009) A639.
[17] S. Muto, Y. Sasano, K. Tatsumi, T. Sasaki, K. Horibuchi, Y. Takeuchi, Y. Ukyo, J. Electrochem. Soc. 156 (2009) A371.
[18] Y. Itou, Y. Ukyo, J. Power Sources 146 (2005) 39.
[19] H. Zhang, C. Sun, F. Li, C. Liu, J. Tan, H. Cheng, J. Phys. Chem. C 111 (2007) 4740.
[20] J.A. Collins, Failure of Materials in Mechanical Design, John Wiley, New York, 1993.
[21] V. Tvergaard, Adv. Appl. Mech. 27 (1990) 83.
[22] M. Monthioux, B. Smith, B. Burteaux, A. Claye, J. Fischer, D. Luzzi, Carbon 39 (2001) 1251.
[23] S.C. Mayo, P.R. Miller, J. Sheffield-Parker, T. Gureyev, S.W. Wilkins, Attainment of <60 nm Resolution in Phase-Contrast X-ray Microscopy using an add-on to an SEM, 8th International Conference on X-ray Microscopy, IPAP Conference Series, 2005, pp. 343–345.
[24] P. Mainwaring, Microsc. Today 16 (6) (2008) 14.
[25] L. Shen, Z. Chen, Chem. Eng. Sci. 62 (2007) 3748.
[26] B. Munch, L. Holzer, J. Am. Ceram. Soc. 91 (12) (2008) 4059.
[27] E. Bullitt, G. Gerig, S.M. Pizer, W. Lin, S.R. Aylward, IEEE Trans. Med. Imaging 22 (2003) 1163.
[28] D. Gostovic, J. Smith, D. Kundinger, K. Jones, E. Wachsman, Electrochem. Solid-State Lett. 10 (2007) B214.
[29] F.C. Walsh, A First Course in Electrochemical Engineering, The Electrochemical Consultancy, Romsey, Hants, UK, 1993.